Controlled Large-Area Lithium Deposition to Reduce Swelling of High-Energy Lithium Metal Pouch Cells in Liquid Electrolytes

Jie Xiao

jie.xiao@pnnl.gov

Pacific Northwest National Laboratory https://orcid.org/0000-0002-5520-5439

Dianying Liu

Pacific Northwest National Laboratory

Bingbin Wu

Pacific Northwest National Laboratory

Yaobin Xu

Pacific Northwest National Laboratory https://orcid.org/0000-0002-9945-3514

Jacob Ellis

Pacific Northwest National Laboratory

Arthur Baranovski

Pacific Northwest National Laboratory

Dongping Lu

Pacific Northwest National Laboratory

Joshua Lochala

Pacific Northwest National Laboratory https://orcid.org/0000-0001-5325-4416

Cassidy Anderson

Pacific Northwest National Laboratory

Kevin Baar

Pacific Northwest National Laboratory

Deyang Qu

University of Wisconsin Milwaukee https://orcid.org/0000-0003-3413-6574

Jihui Yang

University of Washington https://orcid.org/0000-0002-5022-1771

Diego Aranda

Texas A&M University

Katherine Lopez

Texas A&M University

Perla Balbuena

Texas A&M University

Jorge Seminario

Texas A&M University https://orcid.org/0000-0001-5397-9281

Jun Liu

Pacific Northwest National Laboratory https://orcid.org/0000-0001-8663-7771

Article

Keywords:

Posted Date: August 16th, 2023

DOI: https://doi.org/10.21203/rs.3.rs-3256630/v1

Additional Declarations: There is **NO** Competing Interest.

Version of Record: A version of this preprint was published at Nature Energy on March 21st, 2024. See the published version at https://doi.org/10.1038/s41560-024-01488-9.

Controlled Large-Area Lithium Deposition to Reduce Swelling of High-Energy Lithium Meta l Pouch Cells in Liquid Electrolytes

Dianying Liu,[1,†] Bingbin Wu,[1,†] Yaobin Xu,[1] Jacob Ellis,[1] Arthur Baranovskiy,[1] Dongping Lu,[1] Joshua Lochala,[1] Cassidy Anderson,[1] Kevin Baar,[1] Deyang Qu,[2] Jihui Yang,[3] Diego Galvez-Aranda,[4] Katherine-Jaime Lopez,[4] Perla B. Balbuena,[4] Jorge M. Seminario,[4] Jun Liu[*,1,3] and Jie Xiao[*,1,3]

[1]Pacific Northwest National Laboratory, Richland, WA99352, United States
[2]University of Wisconsin Milwaukee, Milwaukee, WI53211, United States
[3]University of Washington, Seattle, WA98122, United States
[4]Texas A&M University, College Station, TX77843, United States
†: These authors contributed equally to this work

Corresponding authors: jie.xiao@pnnl.gov, Jun.liu@pnnl.gov

Abstract:

Lithium (Li) metal battery technology has attracted world-wide attention because of its high energy density, but its practical application is hindered by several challenges, with one significant issue being the large volume change and cell swelling. While external pressure is known to have a profound effect on cell performance, there are currently no reports exploring the relationship between external pressure and the electroplating of Li^+ in large-format pouch cells to enhance overall performance. Here we investigate the influence of externally applied pressure on the electroplating and stripping of lithium metal in 350 Wh/kg pouch cells. A hybrid constant gap and constant pressure design is designed to apply a minimal external pressure for practical application. The self-generated pressures are monitored and quantified which are further correlated to the observed charge-discharge processes. A two-stage cycling process is observed. In the first stage, Li^+ ions utilized are mainly supplied by the cathode which shuttle between the cathode and anode with minimal Li loss which minimizes cell swelling but only happens when pressure is applied appropriately. In the second stage, Li from the Li foil anode participates in the reaction and the thickness of the anode gradually increases. However, even after extensive cycling, cell swelling remains less than 10%, comparable to that of state-of-the-art Li-ion batteries. In addition, the pressure distribution along the horizontal direction across the surface of Li metal pouch cell reveals a complex behavior of Li^+ migration during the electroplating (charge) process. The external pressure encourages a preferred plating process of Li in the central region, necessitating the development of new strategies to address uneven Li plating and utilization to advance Li metal battery technology.

Main

Rechargeable lithium (Li) metal batteries have recently gained significant interest due to their potential to double the cell-level energy of state-of-the-art lithium-ion batteries [1]. Great progress has been made in both fundamental understanding of lithium dendrite formation [2], interfacial

reactions [3,4], and cell failure mechanisms [5,6] and in increasing cell-level energy and cycling stability [7,8]. Key parameters, including the electrolyte amount, cathode mass loading, and lithium metal thickness, have been identified as crucial factors that dictate the cycling stability of lithium metal coin cells [3]. These parameters must be carefully controlled to achieve meaningful results during coin cell testing and enable fair comparisons [9,10].

However, practical applications of high-energy Li batteries are still hindered by several significant challenges. Despite the great progress on the design and fabrication of practical high-energy pouch cells [8], the cycle life needs to be further improved. Another significant challenge is the large volumetric change of the anode and subsequent cell swelling. For practical applications, the cell swelling needs to be limited to less than 10% [11,12]. Most modern Li-ion batteries with metal oxide intercalation cathodes and graphite anodes can meet this requirement [13-15]. For Li cells, the lithium metal is repeatedly deposited on and stripped from the anode, and the morphology of the electrode becomes increasingly porous, causing significant cell swelling. The degree of cell swelling depends on the cell chemistry and cell parameters, typically ranging from 50% to more than 100% [7] for Li metal pouch cells. Even with a compatible electrolyte, the cell swelling is still between 20% to 50% [8]. Such a large cell swelling can be a key reason for cell failure and cannot be tolerated for practical applications. External pressure has been playing a critical role on the electrochemical processes of lithium metal [16,17]. External pressure is known to significantly enhance the cycling stability of all solid-state lithium metal cells and shape the morphology of the deposited lithium metal [18]. For lithium metal cells using liquid electrolyte, there have been several reports discussing the impact of external pressure on coin cells [19,20], single-layer pouch cells [21,22], or small anode-free pouch cells [16,23]. These investigations suggest that the external pressure can influence the structure of the solid electrolyte interphase (SEI) layers and is beneficial for achieving long cycle life.

However, to date, there have been no reports to understand the role of pressure on practical, large-format high-energy Li metal batteries, leaving key questions unanswered. Findings from small areas in coin cells can significantly differ from those in large-format electrodes, as the surface roughness of electroplated Li (and any other metal) becomes worse with increasing plating area [2]. For high-energy Li metal pouch cells, it remains unknown how the pressure stabilizes the cell performance and whether the pressure or electrolyte amount plays the dominant role in determining the cycle life. Achieving a high energy density pouch cell often involves using a lean electrolyte, raising questions about how external pressure affects both the electrolyte distribution and the utilization of lithium metal within pouch cells.

This work utilizes three identical 350 Wh/kg lithium metal pouch cells to investigate the fundamental relationship between pressure and the electroplating process of lithium metal. Different external pressures are compared and correlated to the performance of these pouch cells. The long-term cycling cell swelling is reduced from more than 20-40% in the previous studies to less than 6-8% in this work, which is now comparable to that of state-of-the-art Li-ion batteries. A two-step utilization of Li stored in NMC and Li foil anode are discovered which explains the substantial decrease of cell swelling. Additionally, the pressure distribution on the pouch cell surface is mapped to understand the reaction activity across the entire cell surface during cycling, revealing a Li^+ detour phenomenon leading to preferred plating of Li in the central area of anode. New strategies are needed to extend the region of minimum swelling and mitigate the edge effect to further improve the cell performance.

Results and Discussion

There are two common designs for applying external pressures on Li-ion pouch cells [24]: constant gap or constant pressure. The former involves fixing a cell between two plates, which restricts outward expansion (Fig. S1a and 1d), while the latter typically adds constant spring force between two plates (Fig. S1b and 1e). The "brace" design of constant gap works effectively for Li-ion batteries due to the limited volume change of intercalation compounds used in Li-ion batteries. In the case of lithium metal cells, the volume change during charge is substantial, especially when multiple layers of Li foils are stacked within the same cell. As a result, the screws used to secure the two plates in the constant gap design get pushed up by the expanded cell, creating additional gaps between the plates during cycling. Therefore, more rigid enclosures are required to secure the lithium metal pouch cell [16]. In the constant pressure design, the addition of four springs (Fig. S1b) on top of the two brace plates helps maintain the pressure or force within a fixed range, depending on spring constant. By selecting appropriate springs, the deflection can be minimized, thereby maintaining an almost "constant" pressure on Li-ion pouch cells. However, due to the larger volume expansion of Li metal batteries compared to Li-ion batteries during cycling, the deflection of the spring cannot be minimized by solely using the "constant pressure" fixture depicted in Figure S1b for Li metal pouch cells.

In this work, a modified testing fixture is designed (Fig. S1c and 1f) which combines both constant gap and constant pressure. It includes an additional modified bolt in the center of the "constant pressure" brace. This hybrid fixture allows the cell to expand and the spring to deflect while limiting its movement along the length of the bolt. As a result, a relatively consistent pressure is maintained during most of the cycles, potentially preventing significant volume increase at the end of the charge.

Three identical Li metal pouch cells were prepared using the same cell parameters, each with a total cell-level energy of 350 Wh/kg (see Table S1, cell design A for details). The three key parameters affecting lithium metal battery cycling stability were kept consistent in all three pouch cells: (1) Li anode thickness of 50 μm on each side of the copper current collector, (2) $LiNi_{0.6}Mn_{0.2}Co_{0.2}O_2$ (NMC622) cathode with a mass loading of 19.1 mg/cm^2 corresponding to 3.5 mAh/cm^2 of areal capacity on each side of the aluminum current collector, and (3) an electrolyte amount of 1.9 g/Ah in all cells. Without precise control of these three key parameters, it is challenging to develop a conclusive understanding of the impacts of pressure.

In all pouch cells, the self-generated pressures (blue lines in Fig. 1a-1c) increase during charge due to the plating of additional Li metal layers on the anode side. It is important to note that in Li/NMC622 chemistry, Li^+ ions are stored in two different reservoirs, NMC cathode and the Li foil anode. Li from NMC cathode is used for plating during charge and stripping during discharge, while the original 50 μm Li foil initially functions as a lithium reservoir and current collector before the Li from the cathode is "depleted". The self-generated pressure decreases during discharge as Li is stripped and travels back to the cathode lattice sites. The magnitude of changes in self-generated pressure is inversely related to the externally applied pressure on the fresh pouch cells. When applying pressures of 16 and 26 psi, the peak pressures at the end of the first charge reach 140 and 120 psi, respectively (Fig. 1a and 1b). However, when applying 36 psi to the pouch cell, the highest self-generated pressure is only 70 psi at the end of the first charge (Fig. 1c).

Correspondingly, a relatively high initial pressure leads to the reduced amplitude of maximum pressure observed during each charge (Fig. 1d-1f).

During cycling, the pressure at the end of charge increases almost every cycle (Fig. 1d-1f) in all three pouch cells, indicating continuous "thickening" of the anode. Surprisingly, the pressures at the end of each discharge (Fig. 1d-1f) show almost no change in the first 50-100 cycles (under 16 or 26 psi, Fig. 1d and 1e), or even 250 cycles (under 36 psi, Fig. 1f), and usually return to the originally applied value. This result suggests that in the first tens or hundreds of cycles (depending on the external pressure), there is barely cell thickening at the end of discharge. The only explanation for this observation is that during this period, most of the Li being utilized comes from the NMC cathode which are reversible between two electrodes. During the charge and discharge process, the Li from the cathode shuttles between the cathode and anode with minimum Li loss on the anode, similar as what happens in a traditional lithium-ion cell. The higher initial pressure reduces the irreversible loss of Li during each cycle because most of the Li (from NMC) can return to cathode, resulting in almost full recovery of the initial pressure observed at the end of discharge. During this period, the Li foil is almost intact and functions primarily as a current collector (SEM images). At the same time, very limited cell swelling happens. The discovery of "Li shuttling" phase is very important providing a new perspective to lithium metal batteries if such a stable phase can be further extended.

For Li^+ ions stored in original Li foil side, they gradually become involved in the electrochemical and chemical reactions upon cycling. This is reflected in the continuous increase of end-of-charge pressure after each cycle due to anode thickening. Pressures at the end of charge and discharge steadily increase, particularly towards the end of cycling. Nevertheless, the amplitude of pressure increase from the beginning to the end is always lower in the pouch cell tested with higher externally applied pressures. It is worth noting that for liquid cells, applying a high external pressure does not necessarily translate to better performance. Higher external pressure also increases the probability of an internal short (Fig. S2) proportional to the defective sites in the cell, such as those near the tabbing area [25], especially under elevated pressures. Notably, the highest pressure used in this work, 36 psi, is considerably lower than the range of 2 MPa to 250 MPa (290 psi to 36259 psi) used for solid-state lithium metal batteries [26-28].

It is also surprising that the cycling stability of the three pouch cells under different initial pressures does not exhibit significant differences. The cell under 16 psi experiences a capacity degradation to 80% of its original capacity after 282 cycles (Fig. 1g). The pouch cells under 26 and 36 psi reach 80% of their initial capacity after 299 (Fig. 1h) and 318 cycles (Fig. 1i), respectively. To understand this, it is necessary to consider the dominant factors influencing the cycling stability of Li metal batteries at different stages. As mentioned earlier, several parameters impact the cycling of Li metal cells, such as cathode loading, Li thickness, and electrolyte amount. From the current results, limited external pressure (again external pressure cannot be too high in order to avoid internal short) does not significantly extend the cycling performance of lithium metal batteries if the liquid electrolyte almost dries out. In liquid cells, the amount of available electrolyte dominantly determines how long a Li metal battery last. Once the electrolyte is depleted, the nearly "dried" cell does not respond effectively to this minimal external pressure, resulting in similar cycle life (Fig. 1g-1i) among all cells at different pressures. Another 350 Wh/kg pouch cell with an increased amount of electrolyte of 2.2 g/Ah (compared to 1.9 g/Ah in this work) demonstrated

approximately 459 stable cycles (Fig. S3 and cell design B in Table S1), confirming that the amount of electrolyte plays a more critical role than external pressure in extending the cycle life of Li metal batteries utilizing liquid electrolyte. In our previous published work using a 350 Wh/kg pouch cell with 50 µm Li, which also contained 2.2 g/Ah electrolyte, 430 stable cycles were achieved [8]. Therefore, external pressure only aids in extending the cycling of Li metal when there is still enough liquid electrolyte available in the cell.

The utilization of Li at different stages is summarized in Figure 2. There are two different Li reservoirs in Li/NMC pouch cells, one is in NMC lattice while the second is the original Li foil anode assembled in the cell. In the early stage of the charge-discharge process, Li^+ ions from the NMC cathode shuttle back and forth between the cathode and anode. There is very limited cell swelling at the end of the discharge state because most of Li^+ ions from NMC can reversibly go back to cathode (Fig. 2a). As cycling goes on, more Li^+ ions from NMC are irreversibly lost, Li stored in the foil needs to participate in the electrochemical reaction if there is still enough electrolyte (Fig. 2b). During the second stage of cell cycling, as Li^+ from the Li foil anode begins to participate in the reaction, the thickness of the entire anode gradually increases because Li foil becomes porous accompanied by dead Li and SEI accumulation. Once the electrolyte is depleted, a rapid capacity decay is typically observed (Fig. 2c).

The hybrid constant gap-pressure design greatly reduces cell swelling in all three pouch cells after extensive cycling (Fig. 3). Overall, the pouch cell swelling after extensive cycling is reduced from 20-40% in the previous studies to less than 6-8%, comparable to that of state-of-the-art Li-ion batteries. Prior to cycling, the pouch cell had a measured thickness of 5.45 mm (Fig. 3a). Even under the lowest pressure of 16 psi, cell swelling is only 8.2% after 304 cycles (Fig. 3b). The other two pouch cells under 26 and 36 psi external pressures expand by only 6-7% after more than 300 cycles (Fig. 3c-3d). Appropriate external pressure, combined with a balanced cell design, effectively suppresses the aggressive volume expansion of the Li metal pouch cell during cycling. The cycled lithium metal anodes harvested from three pouch cells are further compared in Figure 3e-3g. The pouch cells were in a discharge state before disassembly, meaning the majority of Li from NMC side returns to the cathode. Figure 3e-3j mainly characterizes cycled Li foil. Intact dense Li is present in all three cycled pouch cells. For consistency, the characterized Li is taken from the same location in the three cells, as indicated in Figure 3k. Some unreacted Li forms column-like structures extending from the current collector to the surfaces of the Li anode, suggesting that the entire Li pillar did not undergo any reaction (Fig. 3e-3g). These unused Li columns are commonly found on the anode side in all three cycled pouch cells (see surface views in Fig. 3h-3j). But the populations of intact Li columns are different on the edges and in the center of the Li foil, which will be discussed in a later section (Fig. 4). It has been observed that after extensive cycling, the thickness of the cycled Li foil also increases, including the intact Li columns, which, in some cases, become even thicker than 50 µm (Fig. 3e and Fig. 3f). These unreacted Li columns are affected by the adjacent Li undergoing dense-to-porous conversion. Under external pressures, intact Li columns elongates beyond their original 50 µm length. After extensive cycling, the SEI and reacted porous Li are entangled forming porous structures in all cycled pouch cells (Fig. S4).

The discussion above focuses on the overall response of the entire pouch cell to the external pressures applied vertically on the cell. The change of self-generated pressures are average values

detected from the pouch cell upon cycling, which are created through changes of all the layers assembled in the battery. How the pressure is distributed across the surface of the pouch cells and its implications of large-scale electroplating of Li are still unknown. To investigate this question, a pressure mapping system (see Methods for experimental setup) was employed to monitor the pressure distribution on the surface of a 350 Wh/kg pouch cell (Fig. 4 and Fig. S5). After a resting period of 2 hours at open circuit voltage, the average pressure on the cell surfaces was measured to be 32.7 psi (Fig. 4a).

At the end of the first charge (Fig. 4b), the average pressure on the cell surfaces increased to 81.4 psi due to the plating of Li (from NMC) on the anode side. The pressure distribution at the end of the first charge does not follow the same pattern at OCV, and more hotspots are observed in the center (Fig. 4b) which is further amplified at the end of the 5^{th} (Fig. 4c) and 20^{th} charge (Fig. 4d). At the end of 50^{th} (Fig. 4e) and 100^{th} (Fig. 4f) charge, the hotspots propagate to the rest regions of cell surfaces, suggesting the availability of more active areas within the cells.

The pressure distribution at the end of discharge (Fig. 4g-4k) follows a similar trend, but the magnitude of pressure increase at the end of discharge is much lower compared to the end of charge, consistent with our earlier discussions. For example, at the end of the first discharge, when the plated Li (from NMC side) returns to the cathode, the average surface pressure reverts back to 34 psi, close to the OCV value of 32.7 psi (Fig. 4g). As cycling progresses, the average surface pressure at the end of discharge increases with small amplitude (Fig. 4g-4k), indicating the presence of residual materials after each cycle, such as entangled SEI and dead Li. The atomic ratio of different elements (C, N, F, O, S, Li, Ni, Mn, Co) and components of SEI on the Li anode at various locations (near-tab area, center, side, bottom) of electrode under different pressures (16 psi, 26 psi, 36 psi) do not exhibit significant differences, suggesting that external pressure, at least within the range discussed in this study, pressure does not impact the SEI formation process notably (Fig. S6-Fig. S7).

Each time when reaching the end of the charge, it has been observed that the amplitude of pressure increase in the central part of the pouch cell is consistently higher than in the rest of the regions on the same surface. This indicates that more significant "thickening" occurs in the center of the anode. To understand this phenomenon, the pressure mapping on the cell surface was stopped after about 100 cycles for post-mortem analysis. A representative Li metal anode from the cycled pouch cell is shown in Figure 4l. In all harvested Li metal foils from the cell, the center part of the cycled lithium anode consistently appears shinier than the four edges (Fig. 4l). Unreacted dense Li columns (highlighted in Fig. 4m-4p) are generally observed in all four selected regions from the cycled Li (Fig. 4l), but the population of intact Li columns varies at different locations. The central part of the Li anode contains more intact Li (Fig. 4m) compared to the edges (Fig. 4n-4p), which aligns with the color difference observed (Fig. 4l). This suggests that less Li in the center area is involved in electrochemical reactions, thus maintaining a dense morphology and metallic shine better than the rest of the Li foil. This observation is common when examining both sides of the same cycled Li foil (Fig. S8) as well as different Li foil anodes from the same pouch cell (Fig. S9 and S10). Even after 300 cycles, harvested Li foils from the Li metal pouch cells in Figure 3 exhibit similar attributes to those seen in Figure 4l, with the center part being much brighter than the rest of the Li foils (Fig. S11), confirming that the consumption of Li in the center is slower than at the edges.

The presence of more intact and shinier Li in the center part seems contradictory to the significant increase in pressure detected in the center of the pouch cell (Fig. 4e and 4f). Note that the accelerated pressure increase in the central part of pouch cell happens during charge meaning Li from NMC is covering anode surfaces. The pouch cells used for analysis, however, are all disassembled in discharged status with the majority of Li from NMC already traveling back to cathode. The less utilization of center Li foil indicates that the majority of Li involved in the electrochemical reactions occurring in the central part of cell is from NMC side. Li originally "stored" on the edges of the Li foil participates more in the cycling compared with the central Li.

Li^+ detour mechanism is proposed here to explain the observed phenomenon and illustrated in Figure 5a. During charge, Li (from NMC) is not homogeneously plated on the Li foil anode side. Instead, Li^+ ions (from NMC) preferably plate in the center of Li foil anode leading to the much faster increase of self-generated pressure in the central area of the pouch cell. Ideally, the electroplating of Li (from NMC) should follow the ideal process in Figure 2. However, impacted by external pressure, some of the Li^+ ions that are supposed to deposit on the edges now detour to the center of Li anode and are plated there, leading to a thicker deposition layer in the central area of anode and thus higher pressure from that region. During the subsequent discharge process, more Li on the edges of Li foil anode participates in the electrochemical reaction due to less coverage by electroplated Li layers compared to the central Li foil that is better "protected" by the Li deposits from the NMC side. After repeated cycling, the utilization and darkening of Li occur earlier on the edges than in the central region of the original Li foil. To prove the Li detour hypothesis, a single layer pouch cell is charged and disassembled at the charge status after 3 cycles (Fig. 5b and Fig.S12a) and 100 cycles (Fig.5c and Fig.S12b). In contrast to those cells disassembled in discharge status, this time the central area is much darker than the edges of Li anode indicating more nano particles of Li are plated in the center anode during charge.

In another parallel 350 Wh/kg Li metal pouch cell, cycling was continued for over 300 cycles (Fig. S13). Significant pressure increase was observed across the entire cell surface, still with the highest pressure concentrated in the central area. This phenomenon is similar to the pressure mapping results observed in Si-based pouch cells[29], although a different pressure fixture was used. Towards the end of the cycling, the pressure distribution on the surface of the pouch cell stabilized with minimal changes. The pressure mapping images at the 300^{th} and 309^{th} cycles (inset of Fig. S13) displayed almost identical pressure distribution and amplitudes, confirming that the electrolyte had almost completely dried out after 300 cycles. Limited external pressure does not extend the cycling of the "dried" cell towards the end of cycling.

Ab Initio Electric Fields:

To gain a deeper understanding of the Li^+ detour phenomenon during electroplating, we have calculated with ab initio electronic structure methods based on density functional theory, the electrostatic potentials (EP) and electric fields (EF) induced on the neighborhood of the surface of Li metal tablets representing structures at different applied pressures, and thus having different concentrations of Li-nuclei (supplement). We also calculated the EPs and EFs on a larger tablet containing two different nuclei concentrations: a high one around the center of the tablet and a lower one around the peripheral of the tablet (Fig. 5d).

The specific movement of chemical species in any type of material (containing nuclei and electrons) can be studied using the electric field ($\mathscr{E}$), i.e., the force per unit of charge, created internally by the same system components in addition to the internal fields. The electric field, mainly, tells the magnitude and direction of the displacements of charged moieties (ions and counterions), as well as the rotational movement of neutral dipolar molecules (such as solvents and additives) to align their electric dipole in the direction of the electric field.

To directly demonstrate the effects of a non-uniform pressure, we analyzed a slab having two different concentrations of Li nuclei (Fig. 5d). The full slab has an area of 3L×3L, with 3L = 2.6 nm. The area of the highest concentration site is a square of L×L sitting in the center of the 3Lx3L surface. The remainder of the surface has a lower concentration of Li nuclei. Figure 5d shows the lines of electric field (blue) originated by the Li-metal surface. They only represent the direction of the trajectories. The values of the electric field are indicated with an orange background in the most representative places approaching the anode and the electric potential of the black iso-potential contours appear with a green background. The low Li concentration at the left- and right-side surfaces show a repulsive behavior against Li-ions and the central one at high pressure features a much higher attraction, even attracting any Li-ion positioned above the low-pressure sites.

We conclude that the driving forces producing the observed trajectory deflection near the anode surface could be determined or controlled by the pressure applied to the pouch cell, increasing the concentration of Li nuclei in the anode, and triggering further electric field changes that drive more Li^+ ions near the anode to the high-concentration or high-pressure zones of the anode. These induced electric fields in the vicinity of the anode arise from the quantum mechanical effects of the charges carried by the electrons and nuclei of the anode. Therefore, ab initio results provide valuable insights into utilizing external pressure to facilitate preferred deposition in specific anode regions, and such information may be used to optimize the Li deposition and stripping processes.

Conclusions

This study investigates the electrochemical plating of Li^+ on a large scale in realistic 350 Wh/kg Li metal pouch cells under varying pressures. It has been discovered that a higher external pressure helps to enhance the cycling and significantly minimize the cell swelling after extensive cycling. However, the critical role that external pressure plays in extending cell cycle life is only observable when there is still enough electrolyte present in the battery. Mapping the pressure distribution across the surface of the pouch cell during cycling reveals a preferential plating of Li^+ in the central area of the anode side. This intriguing phenomenon of Li^+ detour, influenced by pressure, is explained through precise quantum theory calculations and experimentally validated in a custom-designed Li-free anode-limiting pouch cell, where the cathode area is larger than the anode. These findings shed light on the distinct behaviors of Li^+ during large-scale electrochemical plating driven by pressure and provide valuable insights for developing effective solutions to address challenges in rechargeable Li metal batteries.

Methods

Electrodes/electrolyte preparation

The slurry for the NMC622 cathode (Targray, Canada was prepared by combining 96 wt.% NMC622, 2 wt.% conductive carbon (Super P C65, Timcal), and 2 wt.% polyvinylidene difluoride (PVDF) binder (L1120 from Kureha, Korea) in N-methyl-2-pyrrolidone (NMP) solution. The mixture was thoroughly mixed using a Thinky mixer in a dry room maintained at a constant temperature of 19 °C and a relative humidity of 0.1% (dew point controlled below -55 °C). Additional NMP (Targray, Canada) was added to adjust the solid content to 51 wt%. The slurry was then coated onto both sides of a 10-μm-thick Al foil using a comma coating machine (Mediatech, Korea) to achieve a controlled areal coating weight of 19-20 mg/cm^2 (~3.5 mAh/cm^2). or single layer pouch cells and the outer electrodes of multiple layer pouch cells, a single-side coated NMC622 electrode was prepared. The coated cathode was calendared to 2.8 g/cm^3, punched into rectangular pieces, and dried in a vacuum oven at 60 °C for 24 hours. After drying, the cathode electrode was cut to dimensions of 36.0 mm wide and 54.0 mm long, and any residual NMC622 materials on the Al tab were removed with NMP prior to cell assembly. Free-standing Li foil (50 μm, Li content ≥99.9%) was obtained from China Energy Lithium and used directly in the dry room. The Li foil was laminated onto both sides of a Cu mesh current collector (MTI, USA) in the dry room, and then punched into rectangular pieces. The Li anode electrode was cut to dimensions of 37.5 mm wide and 55.5 mm long prior to cell assembly. Battery-grade lithium bis(fluorosulfonyl)imide (LiFSI) (Nippon Shokubai, Japan) was dried at 120 °C under vacuum for 24 hours before use. 1,1,2,2-tetrafluoroethyl-2,2,3,3-tetrafluoropropyl ether (TTE, 99%, SynQuest Laboratories, USA) was dried with 4Å molecular sieves prior to use. LiFSI and 1,2-dimethoxyethane (DME, Gotion, Inc. China) were mixed together and then diluted with TTE to create a 1.5 M LiFSI–DME–TTE electrolyte solution (with a DME/TTE molar ratio of 1.2:3) in an argon-filled glove box with oxygen and moisture levels below 0.1 ppm.

Pouch cell assembly

All pouch cells were assembled in a dry room with a semi-automated cell manufacturing line (MediaTech, Korea) at the Advanced Battery Facility Lab of the Pacific Northwest National Laboratory (PNNL). The assembly process involved slurry mixing, comma coating, calendaring, Z-stacking of cathode, anode, and separator, grid trimming, ultrasonic welding for connection with Al (cathode) and Ni (anode) external tabs, packaging foil formation, top and side sealing, and vacuum sealing with electrolyte injection. As seen in the cell design in Table S1, to achieve 350 Wh/kg energy density, the areal capacity of NMC622 cathode was controlled to 3.5 mAh/cm^2 on each side of the Al foil. Each pouch cell consisted of 16 layers of double-sided anodes, 15 double-side coated and two single-side coated NMC622 cathode layers. With the 50 μm Li foil, the N/P ratio or cell balance was 3.0:1, and the E/C ratio was 1.9 g/Ah. The total capacity of each pouch cell exceeded 2.1 Ah.

For Li/NMC622 single-layer pouch (SLP) cells, the cathode and anode electrodes were similar as described above for the multi-layer pouch cells. The capacity of the SLP cell was about 160 mAh. The cell configuration (Fig.S12c) comprised of a layer of double-sided Li anode sandwiched with two layers of single side coated NMC622 cathode. Each SLP cell was filled with 1 g of electrolyte. After resting for 24 hours, the SLP cells were clamped using a compression device (as shown in Fig. S1b) with an initial pressure of 36 psi. The initial pressure was measured using a digital force gauge with a remote load cell (SHIMPO FG-7000L, USA). The testing procedure for the SLP cells was same as that for the multiple-layer pouch cells.

In situ pressure test

For the in-situ pressure test, multiple-layer pouch cells were sandwiched in a stainless-steel clamping device (shown in Fig. S1c) with a target initial external pressure. Two silicon mats were placed between the pouch cell and the stainless-steel plates of the clamp to ensure uniform pressure distribution. The pouch cell, along with the in-situ pressure measurement system (Loadstar Sensors, Model: DI-1000UHS, USA), was set in place, and the initial pressure of the cell was adjusted to the target force and fixed with screws. The applied initial force was calculated based on the target pressure and the battery area. For example, when the targeted initial pressure was 16 psi, so the applied initial force was 16 psi * 3.72 $inch^2$ (battery area: 4 cm * 6 cm=24 cm^2=3.72 $inch^2$) = 59.6 lb. The clamped Li metal pouch cells were placed in a gas-detecting safety chamber (Cincinnati Sub-Zero, USA) filled with inert gas (N_2) at 25 °C. Galvanostatic cycling tests were conducted within a voltage range of 2.7 V to 4.4 V using Land battery testers (LANHE CT2001B, China). The pouch cells were first charged/discharged at a constant current rate of 0.1 C for two initial formation cycles, followed by charging at 0.1 C and discharging at 0.3 C in subsequent cycles (1 C corresponds to 3.5 mA/cm^2 or 2.1 A). The in-situ pressure measurement system recorded the force every 10 seconds, and the average pressure was calculated as the average value of all the pressure data points in a cycle.

Pressure mapping test.

For the pressure mapping test, the pouch cell was sandwiched with a clamping device similar to Fig. S1b. Two silicon mats were placed between the pouch cell and the stainless-steel plates of the clamp for uniform pressure distribution. A force mapping sensor (Tekscan, Model 5076, USA) was positioned between the bottom silicon mat and the stainless-steel plate, in contact with the pouch cell. Pressure was applied to the pouch cell until the target pressure of 36 psi or 133.9 lb force was reached. The testing protocol for the pouch cell was the same as the in-situ pressure test. There were slight differences in measurement accuracy between the force mapping sensor and the in-situ pressure measurement system. To make the results from the force mapping sensor relevant to the in-situ pressure measurement system, a calibration was performed. The Tekscan force mapping sensor was calibrated using the Loadstar in-situ pressure measurement system and the SHIMPO digital force gauge. A pressure of 100 psi (or 372 lb force) was applied to the pouch cell, and the average pressure measured by the Tekscan force mapping sensor was recorded. The calibration factor was calculated by dividing the applied pressure (100 psi or 372 lb) by the recorded average pressure from the Tekscan mapping sensor. The average pressure of the pouch cell at a certain voltage during the cycling test was obtained by multiplying the calibration factor by the average pressure provided by the Tekscan force mapping sensor.

SEM/(S)TEM characterization

The surface and cross-section morphology of the cycled Li anodes were characterized using a Thermo Fisher Helios SEM. The cross-sections of the cycled Li anodes were obtained by cutting the anodes with a razor blade in an Ar-filled glove box. The cycled Li anode from the 2 Ah pouch cell at 16 psi was characterized using a 300 kV FEI Titan monochromated (S)TEM equipped with a probe aberration corrector. For the Li metal sample, a Cryo-holder was used to transfer the Li sample to the (S)TEM.

XPS Experimental

XPS measurements were performed using a Thermo Fisher NEXSA system. The system utilized a focused monochromatic Al Kα (1468.7 eV) source for excitation and a double-focusing

hemispherical analyzer with a multi-element input lens and a 128 channel detector. The X-ray beam was incident to the sample at a normal angle, while the photoelectron detector was positioned at a 60° angle relative to the sample normal. High-energy resolution spectra were collected with a pass-energy of 50 eV, a step size of 0.1 eV, and a dwell time of 50 ms. The full-width-at-half-maximum (FWHM) for the Cu 2p3/2 peak was measured to be 0.82 eV under the same conditions used for the collection of the narrow scan spectra.

Ab Initio calculation

The contribution of electrons to generate electric fields can be obtained solving the Schrödinger Equation for a system of n electrons located at points r_i ($r^{(n)}$) and N nuclei located at points R_i ($R^{(N)}$), thus,

$$\widehat{H}\left(r^{(n)}, R^{(N)}\right)\Psi\left(r^{(n)}, R^{(N)}\right) = E\left(R^{(N)}\right)\Psi\left(r^{(n)}, R^{(N)}\right) \quad (1)$$

In this situation, the array of nuclei positions $R^{(N)}$ is directly determined by the pressure applied to the pouch cell, the more pressure the more concentrated the nuclei (Fig. S14). Solving the above equation with an exact Hamiltonian operator ($\widehat{H}$) using ab initio methods such as density functional theory (preferred) or a traditional ab initio (such as HF, MP, CC, CI, etc.), we obtain from this eigenvalue problem the wave function Ψ and the energy E. The wavefunction Ψ yields a Slater determinant that can be written as

$$\Psi = det|\psi_i(r_1)\ \psi_i(r_2)\ \psi_i(r_3)\ \cdots\ \psi_i(r_n)| \quad (2)$$

Where the $\psi_i\left(r_j\right)$ are the crystal or molecular orbitals. In this shorthand notation of the determinant, the rows of the determinant are created running the dummy index i from 1 to n. And the wavefunction is a function of $3n$ variables. For the sake of simplicity, we use atomic units and ignore the n spin variables and normalization constants, but they are considered in the calculations. Thus, the electron density (ρ_e) at any point r can be obtained from summing all occupied orbitals,

$$\rho_e(r) = -\sum_i |\psi_i(r)|^2 \quad (3)$$

And the corresponding nuclei contribution, at points R_i with charges Z_i, using the Dirac δ-function can be written as

$$\rho_N(r) = \sum_i \delta(r - R_i)Z_i \quad (4)$$

These two densities give us the electrical potential at any point r, $V(r)$,

$$V(r) = \int \frac{\rho_N(r) - \rho_e(r)}{|r - r'|} dr \quad (5)$$

Finally, the electric field $\mathscr{E}$ is obtained from the gradient ($\boldsymbol{\nabla}$) of the potential,

$$\mathscr{E}(r) = -\boldsymbol{\nabla}V(r)$$

For a surface under a non-uniform distribution of local pressures, for example a surface with only two of the pressures/concentrations shown in Figure S14, the net electric field in this non-uniform case can be estimated as the vector sum of their corresponding electric fields, since the interactions have been calculated between elementary particles (nuclei and electrons) so their pair interactions are independent of any other particles around. This electric field is obtained through the formalism explained in Equations 1-5 when applied to the nuclei and electrons of the anodes of different densities that can be associated to different applied pressures. Obviously, for this case of having two different pressures on the same surface, the site with the highest pressure will have the highest concentration of lines of force ($\mathscr{E}$). This reasoning can be extended to a surface with any number of different pressures on its surface. We remark that making a larger anode with a given pressure simply adds the electric fields at the center of the anode surface, regardless of the size of the area, and in all cases the electric fields at the lateral boundaries of the anode surface will be mostly repulsive or of reduced attraction with respect to those in the center of the anode.

Acknowledgements

This research has been supported by the Assistant Secretary for Energy Efficiency and Renewable Energy, Office of Vehicle Technologies of the U.S. Department of Energy (DOE) through the Advanced Battery Materials Research Program (Battery500 Consortium). The SEM and TEM were conducted in the William R. Wiley Environmental Molecular Sciences Laboratory (EMSL), a national scientific user facility sponsored by DOE's Office of Biological and Environmental Research and located at Pacific Northwest National Laboratory (PNNL). PNNL is operated by Battelle for the DOE under Contract DE-AC05-76RL01830.

Reference

1 Liu, J. *et al.* Pathways for practical high-energy long-cycling lithium metal batteries. *Nature Energy* **4**, 180-186, (2019).

2 Xiao, J. How lithium dendrites form in liquid batteries. *Science* **366**, 426-427, (2019).

3 Chen, S. *et al.* Critical Parameters for Evaluating Coin Cells and Pouch Cells of Rechargeable Li-Metal Batteries. *Joule* **3**, 1094-1105, (2019).

4 Ren, X. *et al.* Enabling High-Voltage Lithium-Metal Batteries under Practical Conditions. *Joule* **3**, 1662-1676, (2019).

5 Wu, B., Lochala, J., Taverne, T. & Xiao, J. The interplay between solid electrolyte interface (SEI) and dendritic lithium growth. *Nano Energy* **40**, 34-41, (2017).

6 Lu, D. *et al.* Failure Mechanism for Fast-Charged Lithium Metal Batteries with Liquid Electrolytes. *Advanced Energy Materials* **5**, 1400993, (2015).

7 Niu, C. *et al.* High-energy lithium metal pouch cells with limited anode swelling and long stable cycles. *Nature Energy* **4**, 551-559, (2019).

8 Niu, C. *et al.* Balancing interfacial reactions to achieve long cycle life in high-energy lithium metal batteries. *Nature Energy* **6**, 723-732, (2021).

9 Chen, H. *et al.* Free-standing ultrathin lithium metal–graphene oxide host foils with controllable thickness for lithium batteries. *Nature Energy* **6**, 790-798, (2021).

10 Zhang, X.-Q. *et al.* A Sustainable Solid Electrolyte Interphase for High-Energy-Density Lithium Metal Batteries Under Practical Conditions. *Angewandte Chemie International Edition* **59**, 3252-3257, (2020).

11 Zhang, N. & Tang, H. Dissecting anode swelling in commercial lithium-ion batteries. *Journal of Power Sources* **218**, 52-55, (2012).

12 Zhang, N., Tang, H., Zhang, L. & Trifonova, A. Asymmetric Electrode for Suppressing Cell Swelling in Commercial Lithium Ion Batteries. *Journal of The Electrochemical Society* **162**, A2152, (2015).

13 Aufschläger, A. *et al.* High precision measurement of reversible swelling and electrochemical performance of flexibly compressed 5Ah NMC622/graphite lithium-ion pouch cells. *Journal of Energy Storage* **59**, 106483, (2023).

14 Blazek, P. *et al.* Axially and radially inhomogeneous swelling in commercial 18650 Li-ion battery cells. *Journal of Energy Storage* **52**, 104563, (2022).

15 Kalaikkanal, K., Gobinath, N. & Mohan, R. Influence of swelling on the safety aspects of electric vehicle batteries – Short Review. *IOP Conference Series: Earth and Environmental Science* **1161**, 012010, (2023).

16 Louli, A. J. *et al.* Exploring the Impact of Mechanical Pressure on the Performance of Anode-Free Lithium Metal Cells. *Journal of The Electrochemical Society* **166**, A1291, (2019).

17 Louli, A. J. *et al.* Diagnosing and correcting anode-free cell failure via electrolyte and morphological analysis. *Nature Energy* **5**, 693-702, (2020).

18 Fang, C. *et al.* Pressure-tailored lithium deposition and dissolution in lithium metal batteries. *Nature Energy* **6**, 987-994, (2021).

19 Kasse, R. M. *et al.* Combined Effects of Uniform Applied Pressure and Electrolyte Additives in Lithium-Metal Batteries. *ACS Applied Energy Materials* **5**, 8273-8281, (2022).

20 Duan, X. *et al.* Revealing the Intrinsic Uneven Electrochemical Reactions of Li Metal Anode in Ah-Level Laminated Pouch Cells. *Advanced Functional Materials* **33**, 2210669, (2023).
21 Kim, S. *et al.* Correlation of electrochemical and mechanical responses: Differential analysis of rechargeable lithium metal cells. *Journal of Power Sources* **463**, 228180, (2020).
22 Harrison, K. L. *et al.* Effects of Applied Interfacial Pressure on Li-Metal Cycling Performance and Morphology in 4 M LiFSI in DME. *ACS Applied Materials & Interfaces* **13**, 31668-31679, (2021).
23 Genovese, M., Louli, A. J., Weber, R., Hames, S. & Dahn, J. R. Measuring the Coulombic Efficiency of Lithium Metal Cycling in Anode-Free Lithium Metal Batteries. *Journal of The Electrochemical Society* **165**, A3321, (2018).
24 Wünsch, M., Kaufman, J. & Sauer, D. U. Investigation of the influence of different bracing of automotive pouch cells on cyclic liefetime and impedance spectra. *Journal of Energy Storage* **21**, 149-155, (2019).
25 Wu, B. *et al.* Good Practices for Rechargeable Lithium Metal Batteries. *Journal of The Electrochemical Society* **166**, A4141, (2019).
26 Gao, X. *et al.* Solid-state lithium battery cathodes operating at low pressures. *Joule* **6**, 636-646, (2022).
27 Ye, L. & Li, X. A dynamic stability design strategy for lithium metal solid state batteries. *Nature* **593**, 218-222, (2021).
28 Zahiri, B. *et al.* Revealing the role of the cathode–electrolyte interface on solid-state batteries. *Nature Materials* **20**, 1392-1400, (2021).
29 Müller, V. *et al.* Effects of Mechanical Compression on the Aging and the Expansion Behavior of Si/C-Composite|NMC811 in Different Lithium-Ion Battery Cell Formats. *Journal of The Electrochemical Society* **166**, A3796, (2019).

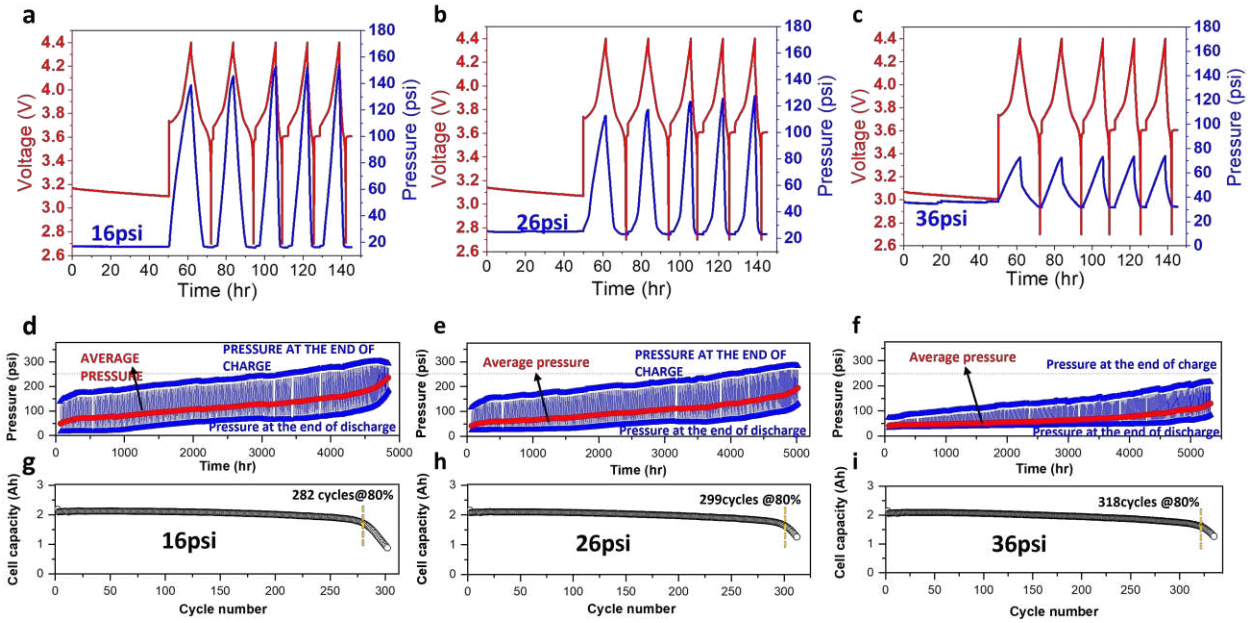

Figure 1. ***In situ*** **pressure monitoring of three 350 Wh/Kg Li/NMC622 pouch cells (2Ah) tested under different initial external pressure: (a, d, g) 16 psi, (b, e, f) 26 psi and (c, f, i) 36 psi. (a-c)** show the evolution of self-generated pressures during charge/discharge for the first five cycles. **(d-f)** compare the pressures detected at the end of charge/discharge for each cycle, highlighting the differences between the pouch cells with varying initial pressures. The average pressure is also plotted in (d-f) to compare the amplitude of pressure change generated by the pouch cells during cycling. **(g-i)** represent the cycling stability of the three Li metal pouch cells tested under different initial pressures: (g) 16 psi, (h) 26 psi and (i) 36 psi. All cells were charged at a rate of 0.1 C and discharged at a rate of 0.3 C between 2.7 V and 4.4 V.

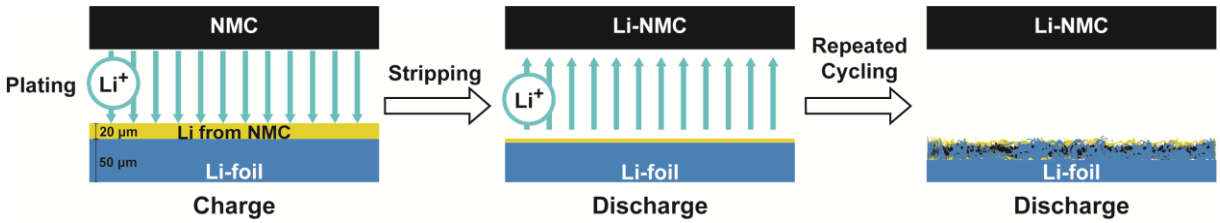

Figure 2. Different stages of Li utilization in a Li/NMC pouch cell. In the initial stage, the Li ions from the cathode is deposited to the anode upon charging. During discharge, the deposited Li goes back to the NMC cathode. Ideally, the Li foil on the anode is not involved much in the reaction in this early stage. As cycling goes on, some of Li from NMC cathode will be lost irreversibly due to forming "dead" Li. Correspondingly, the Li foil begins to participate in the reaction to compensate for the Li loss and more SEI and dead Li are accumulated. In the final stage, the electrolyte is depleted and the cell capacity falls rapidly.

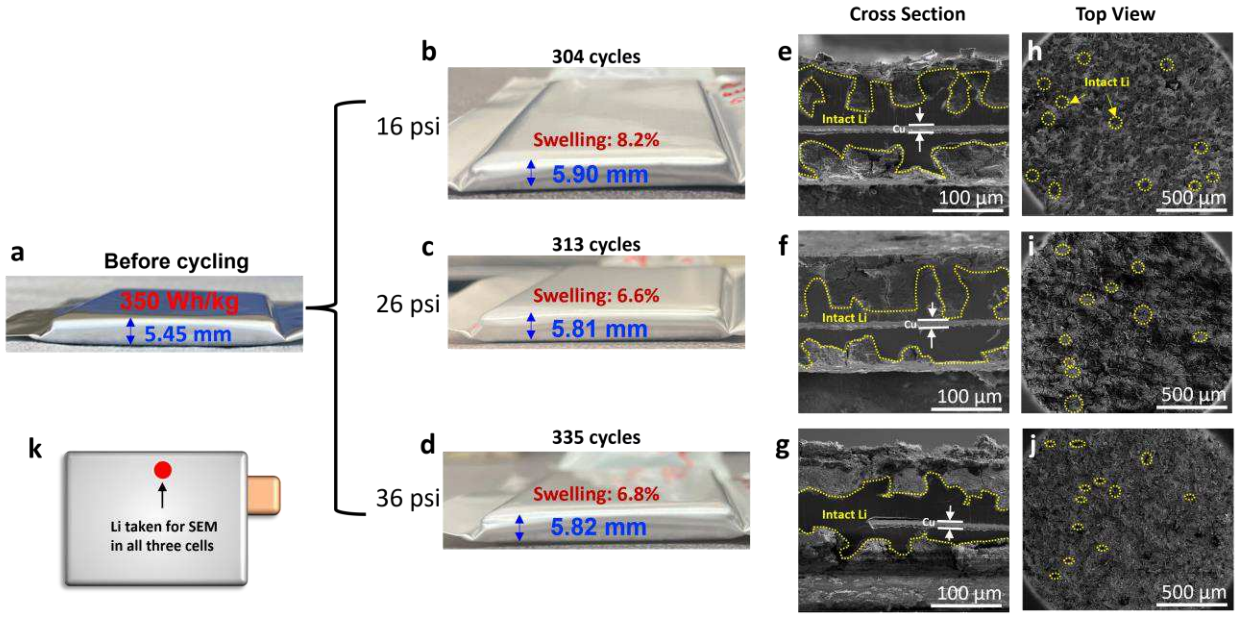

Figure 3. Li metal pouch cells before and after extensive cycling under different initial pressures. **(a)** As-prepared 350 Wh/kg Li metal pouch cell with a thickness of approximately 5.45 mm. **(b-d)** Pictures of pouch cells tested under initial pressures of **(b)** 16 psi after 304 cycles, **(c)** 26 psi after 313 cycles and **(d)** 36 psi after 335 cycles. The swelling rate of all three pouch cells is between 6-8% after extensive cycling. **(e-g)** show cross-section and surface view SEM images of cycled Li metal anodes harvested from pouch cells tested at initial pressures of **(e-h)** 16 psi, **(f-i)** 26 psi and **(g-j)** 36 psi. For each pouch cell, the 5th Li anode assembled in the cell was taken out for further SEM characterization. On each harvested Li anode, a small piece of cycled Li was cut from the same location on the long edge near the copper tab, as indicated in **(k)**.

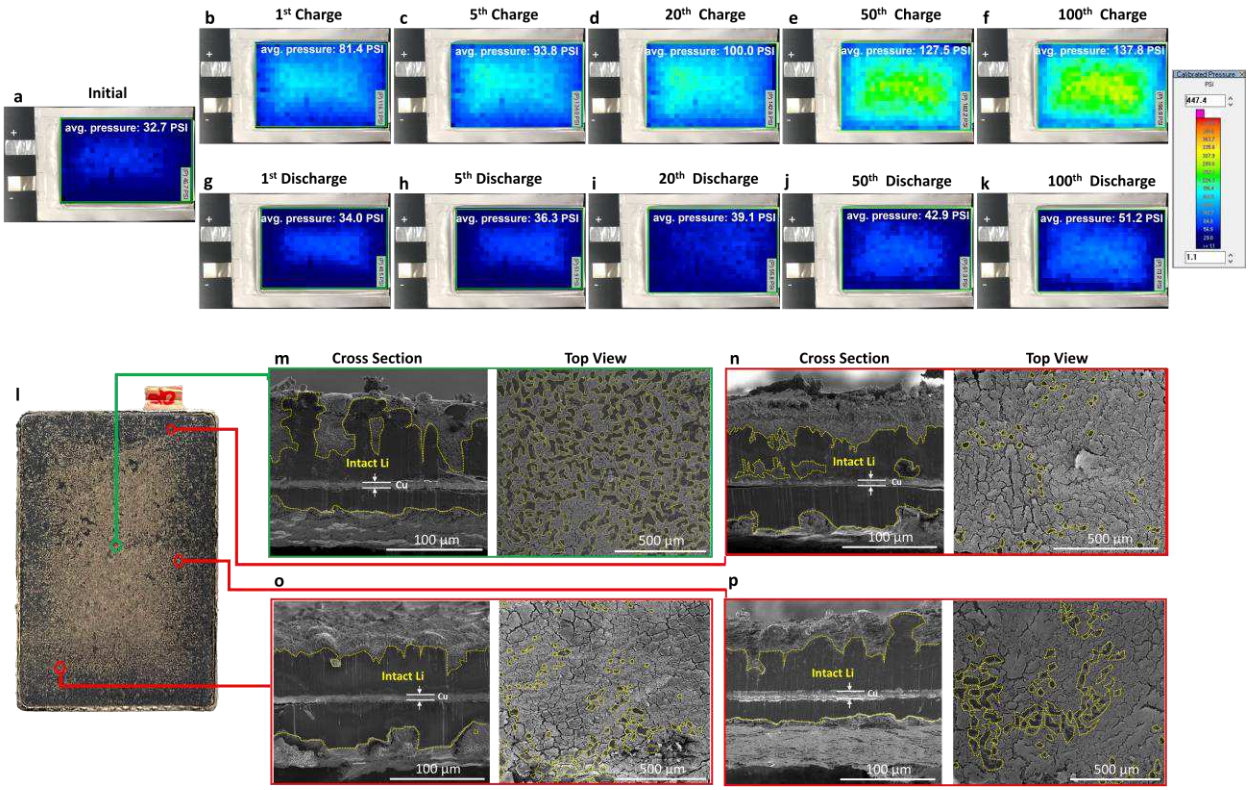

Figure 4. Mapping of pressure distribution on the surface of a prototype 350 Wh/Kg Li/NMC622 pouch cell (2Ah) during cycling and correlation to lithium metal morphologies after cycling. **(a)** The average pressure on the surface of the pouch cell is 32.7 psi at OCV. The pressure applied on the center is slightly higher than the rest area of the pouch cell from the mapping system. Pressure increases continuously on the cell surface after the **(b)** 1st, **(c)** 5th, **(d)** 20th, **(e)** 50th and **(f)** 100th charge. The central part of the pouch cell demonstrates a faster increase in pressure compared to the rest of the surface. Pressure distribution after the **(g)** 1st, **(h)** 5th, **(i)** 20th, **(j)** 50th and **(k)** 100th discharge is also shown. The amplitude of pressure increase on the pouch cell surface is much lower at the end of discharge compared to the charge status. **(l)** is a photo of one of the cycled Li metal anodes harvested from the pouch cell used for pressure mapping. The central part of the cycled Li metal anode maintains its metallic shine and is further analyzed using **(m)** SEM from cross-section and top views. Additional three locations from the edges are also selected for SEM characterizations. **(n)** displays SEM images of Li located on the short edges near copper tab. **(o)** represents the cross-sectional and top view SEM images of Li located in the corner of the cycled Li foil anode, far away from the tabbing. **(p)** shows SEM images of Li located in the long edge of the same Li metal anode as indicated in **(l)**. The pouch cell is in discharge status before being disassembled to harvest the cycled Li metal anode.

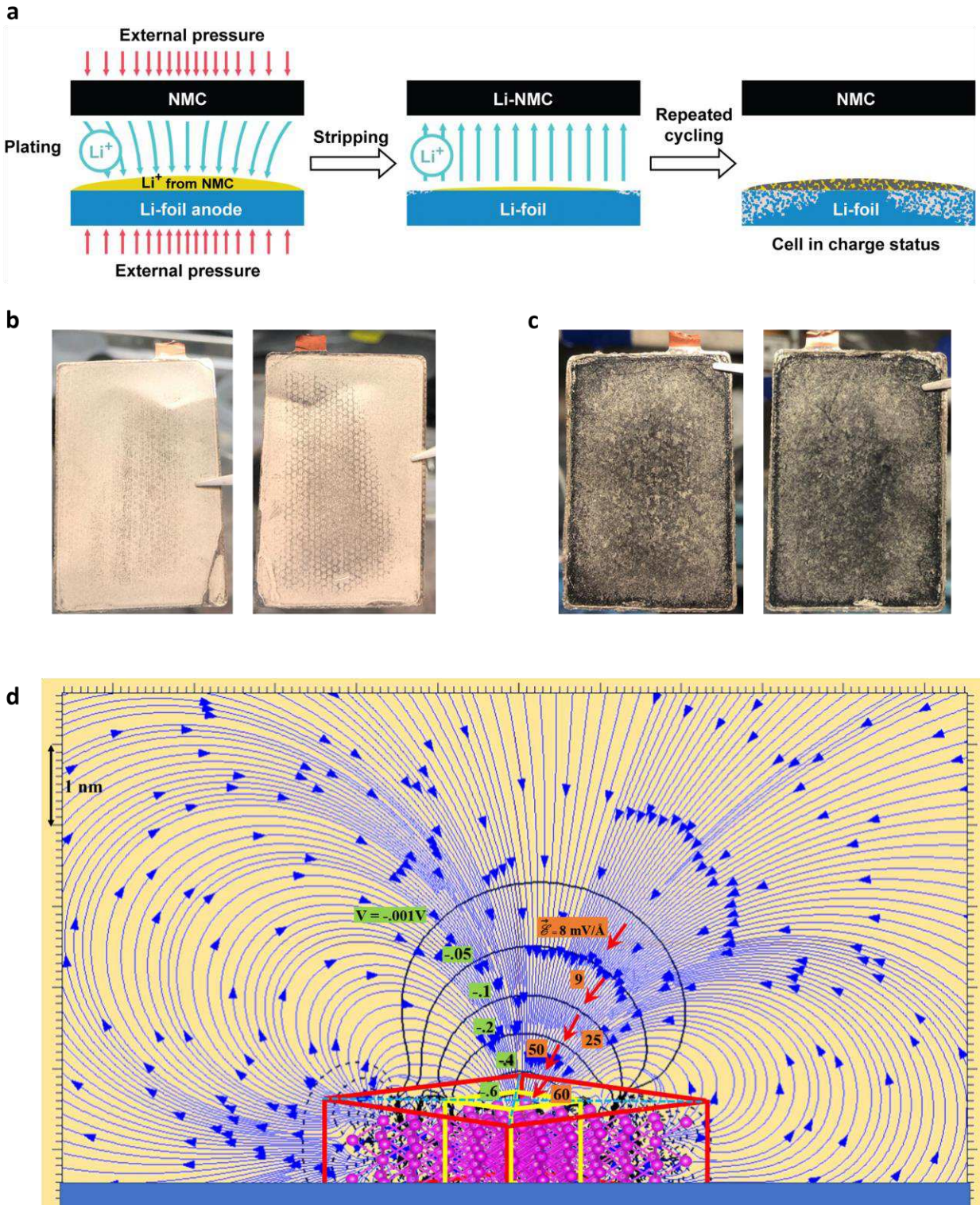

Figure 5. Experimental and theoretical study of Li^+ detour behavior during the electroplating process. **(a)** Visualization of Li^+ detour behavior in Li/NMC pouch cell driven by the uneven distribution of externally applied pressure. **(b-c)** Digital photos of Li anodes harvested from Li metal single-layer pouch

cells (~160 mAh) at charge status after (b) 3 and (c)100 cycles. Both sides of the Li anode are displayed. The single-layer pouch cells were cycled at 0.1 C/0.33 C between 2.7 V and 4.4 V with an initial pressure of 36 psi. They were disassembled at charge status. **(d)** Theoretical calculation of the electric field distribution at the Li anode affected by two different external pressures. The electric field lines of force (blue trajectories) are induced by the nuclei and electrons at the anode, interacting with the incoming lithium ions as they approach the anode, causing deviations from their straight paths due to the charging electric field. The regions of highest concentration or pressure of Li nuclei (yellow cube) are the most attractive to lithium ions. Although this seems to be at odds with Coulombic behavior, it is also clear that a higher concentration of nuclei is accompanied by a higher concentration of electrons in the neighborhood. The red parallelepiped (tablet shape) box is the full anode of Li-metal. The central atoms in the yellow parallelepiped are at a higher concentration (pressure) than the reminder Li-nuclei in the red tablet. The electric potential and the electric field are plotted on a vertical plane that cuts diagonally (on the dashed light blue horizonal diagonal) the red and therefore the yellow parallelepipeds. The electric field values are indicated in an orange background and the electric potentials in a green background.

Supplementary Files

This is a list of supplementary files associated with this preprint. Click to download.

- CellPressureSI.pdf